ACS APPLIED ENERGY MATERIALS
Cite This: ACS Appl. Energy Mater. 2018, 1, 2891−2897
Article
www.acsaem.org

High-Performance Triboelectric Nanogenerator with a Rationally Designed Friction Layer Structure

Nuanyang Cui,[†] Jinmei Liu,[†] Yimin Lei,[†] Long Gu,[†] Qi Xu,[†] Shuhai Liu,[†] and Yong Qin*[,†,‡]

[†]School of Advanced Materials and Nanotechnology, Xidian University, Xi'an 710071, China
[‡]Institute of Nanoscience and Nanotechnology, Lanzhou University, Lanzhou 730000, China

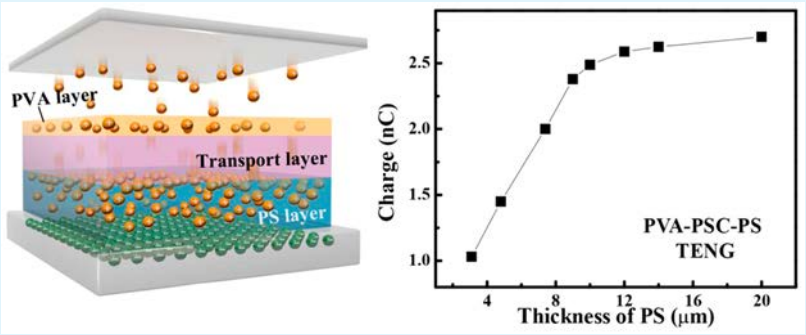

ABSTRACT: For a triboelectric nanogenerator (TENG), its output performance is largely determined by the quantity of triboelectric charge generated on the friction layer during the triboelectrification process. In this paper, we developed a new TENG by designing a three-layered composite structure (TLCS) for the positive friction layer. The TLCS was formed by stacking, from the outermost to the bottom, a charge collection sublayer (CCL), charge transport sublayer (CTL), and charge storage and barrier sublayer (CSBL). The CCL was used for robbing positive charges effectively from the negative friction layer. The CTL was used to transport the generated triboelectric charge deeper inside. The CSBL was used for holding more charges. By fabrication of TLCSs on both the positive and negative friction layers, the total triboelectric charge density increases from 0.97 to 16 nC/cm^2, which greatly enhances the performance of the triboelectric nanogenerator.

KEYWORDS: *triboelectric nanogenerator, composite friction layer, triboelectric charge, PVA, charge storage*

INTRODUCTION

Owing to the fast development of digital information and network technology, a variety of mobile and portable electronics are widely used in daily life. The demand for portable power supplies has become more and more urgent. The current conventional portable power supplies are mainly chemical batteries, such as Li-ion battery, metal−air battery, etc. However, limited by the lifespan and environmental pollution issues,[1] these batteries cannot satisfactorily meet the power requirements of portable electronics. Mechanical energy, as a kind of diversified, widespread, and safe energy, can be found everywhere in the world. If it can be harvested and converted into electricity, it will be an effective way to power portable electric devices. Currently, the piezoelectric effect,[2−11] electromagnetic effect,[12,13] electrostatic effect,[14] and triboelectrification phenomenon have been widely used to scavenge mechanical energy. Among them, triboelectric nanogenerators (TENGs)[15−20] based on the coupling of the triboelectric effect and electrostatic effect have attracted much attention for the high power output and energy conversion efficiency.[21−23] In addition, the strong adaptability makes them applicable in different environments to harvest the mechanical energy in different forms, such as sound waves,[24−26] ambient vibration,[27] body motion,[28] air flow,[29−32] etc.

Since the TENG was invented in 2012, related applications and technology have been developed gradually. In general, the study of the application mainly focuses on developing TENGs for different environments and then establishing corresponding self-powered systems.[33−36] Through the optimization of the overall structure of TENGs, the energy conversion efficiency has been increased to some extent. However, these improvements depend greatly on the specific conditions of the application environment and lack the general adaptability to a wide range of environmental conditions. For example, the optimized design for harvesting sound wave energy is not available for scavenging body motion energy. Improving the performance of the friction layer is one kind of universal method to improve TENG performance. Some works have focused on improving TENG performance by building nano/micro structures on the friction layer surface.[37−39] However, the lack of theoretical analysis is a big stumbling block to further promote the triboelectric charge density in the friction layer.

On the basis of our former work[40] about the analysis of the dynamic behavior of the triboelectric charges in the friction

Received: April 8, 2018
Accepted: May 17, 2018
Published: May 17, 2018

DOI: 10.1021/acsaem.8b00530
ACS Appl. Energy Mater. 2018, 1, 2891−2897

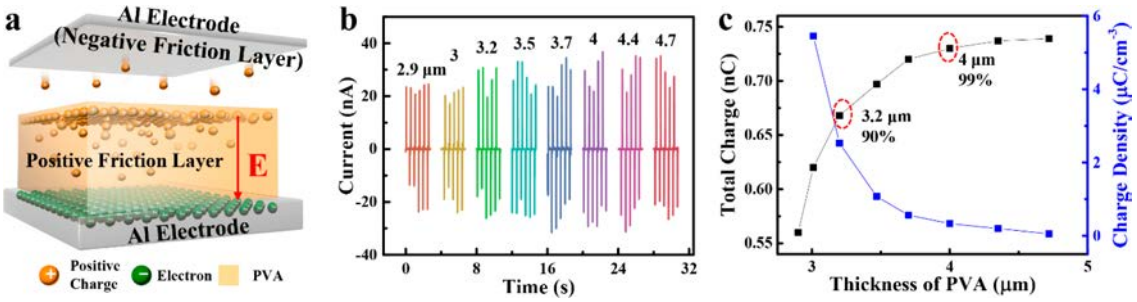

Figure 1. (a) Schematic of the transport process of triboelectric charges in the PVA positive friction layer of TENG. (b) Short-circuit currents of TENG devices with PVA friction layers of different thicknesses. (c) The charge density and total carried charges in different thickness PVA friction layers.

layer, in order to improve the TENG's output, we designed a multilayer composite structure for the positive friction layer. It is composed of a charge collection sublayer (CCL), charge transport sublayer (CTL), and charge storage and barrier sublayer (CSBL) in turn from the surface to the electrode. The CCL can quickly take positive triboelectric charges from the negative friction layer. Under the force of a built-in electric field, built between the positive triboelectric charges in CCL and the negative induced charges in the electrode, these positive charges will migrate to the deeper sublayers through the CTL, and finally remain in the CSBL. In this way, a transport channel is formed and effectively increases the distance between the triboelectric charges and the friction layer surface, which could help to weaken the repulsion between the first entered charges and the positive charges that enter later. This composite structure design increases the charge density by a factor of 3.7 for the TENG's positive friction layer. When this multilayer composite structure is applied in both the negative and the positive friction layer, the charge density can be raised by a factor of 16.5. Our work demonstrates the validity and universality to hold much more positive friction charges by constructing the multilayer composite structure on the positive friction layer in TENGs. This greatly benefits the development of TENG in the future.

■ RESULTS AND DISCUSSION

As demonstrated in previous research,[40] the electrons caught from the positive friction layer will not stay on the surface of the negative friction layer. Instead, it migrates deep inside, driven by the built-in electric field *E*. For the positive charges in the positive friction layer, their dynamic behavior is similar to that of the electrons in the negative friction layer. As shown in Figure 1a, *E* is built between the positive triboelectric charges in the friction layer and the negative induced charges in the electrode. The concentration of positive charges will fall to 0 gradually along the depth of the friction layer, which is determined by the carrier concentration and carrier mobility. To verify this, poly(vinyl alcohol) (PVA) was chosen as the main material for the positive friction layer of the TENG, and the distribution of positive triboelectric charges in PVA layer can be given by testing and analyzing the TENG's output current. The structure schematic of the TENG is shown in Figure 1a. Two poly(methyl methacrylate) (PMMA) plates were selected as substrates, and two pieces of suitable aluminum foils were pasted onto the internal surface of two substrates by double-sided tape. On the aluminum film of the bottom PMMA substrate, a layer of homogeneous and transparent PVA was formed after spin-coating PVA solution and drying it on the hot plate. Here, PVA takes on the role of positive triboelectric material, while the aluminum foil on the bottom substrate was the bottom electrode of the TENG; the aluminum foil on the top substrate acts as both negative triboelectric material and top electrode. Because electrons will not be trapped in the inside of the friction layer, which would allow us to analyze the performance of the positive layer nondisruptively, we choose a conductor as the negative friction layer.

To investigate the distribution of positive charges, a group of TENGs with PVA positive friction layers in different thicknesses were prepared. After being fixed on the linear motor, all these TENGs worked at the same driving force and frequency. In this case, the charge capacity of PVA positive friction layer is mainly related with its thickness and the separation−recombination speed between the positive and negative friction layers is mainly related with its thickness and elasticity. After working for 30 min, the output of these TENGs became very stable and the short-circuit current signals of these devices were collected, as shown in Figure 1b. In this work, the current signal and voltage signal were measured through Stanford Research Systems (low-noise preamplifier SR560 and low-noise current preamplifier SR570). The input resistances of the preamplifiers were 100 MΩ and 10 kΩ, respectively. With the increase of the thickness of the PVA layer, the peak value of the short-circuit current output presents an uptrend basically. However, the individual short-circuit current signals are not enough to demonstrate the charge capacity of PVA, because the current output of a TENG is determined by two factors: the charge quantity carried on the friction layer and the separation−recombination speed between the positive and negative friction layers. Considering that the separation−recombination speed can be reflected in the half-peak bandwidth of the output signals, to demonstrate the charge capacity of the PVA friction layer and remove disturbances from the separation−recombination speed, the short-circuit current curves should be integrated to work out the actual triboelectric charges carried by the PVA friction layer. The calculated total amount of the triboelectric charges is shown in Figure 1c (black line). It can be seen that the charge capacity of the PVA layer continues to increase with the increase of the thickness of PVA layer, but the increasing rate decreases gradually. When taking the volume of these TENGs into account, their volume charge density can be calculated as the ratio of the total triboelectric charge and the volume. The results are shown in Figure 1c (blue line); the volume charge density quickly slows at the beginning and gradually falls away with the increase of the PVA layer's thickness. It can be found

DOI: 10.1021/acsaem.8b00530
ACS Appl. Energy Mater. 2018, 1, 2891−2897

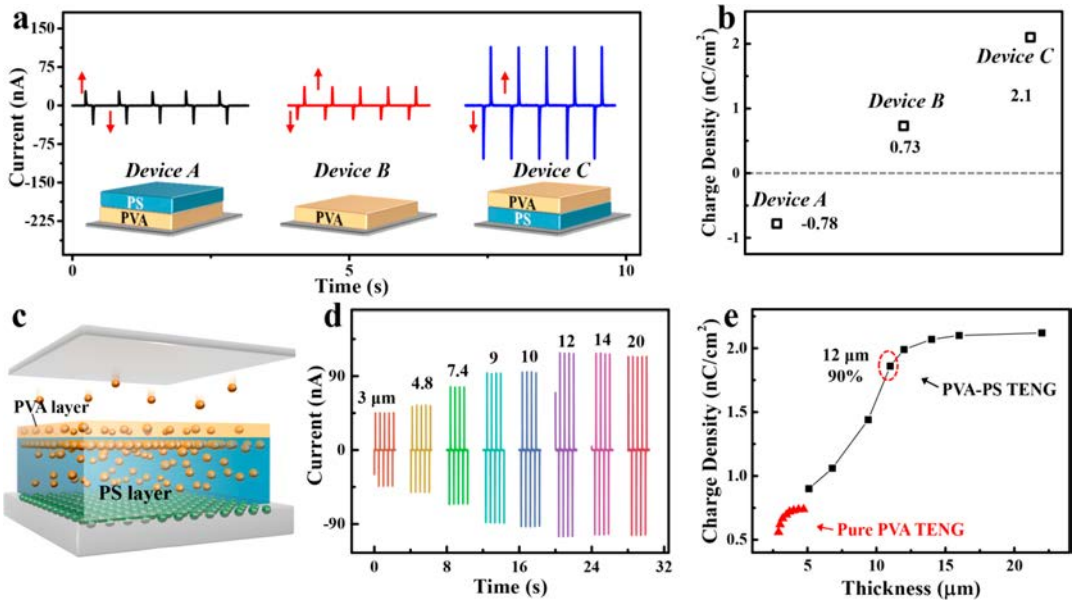

Figure 2. Short-circuit currents (a) and charge density (b) of device A, device B, and device C. Device A has a 20 μm thick PS friction layer and 5 μm thick PVA dielectric layer; device B has 5 μm thick PVA friction layer only, and device C has a 5 μm thick PVA friction layer and 20 μm thick PS dielectric layer. (c) Schematic of the transport process of triboelectric charges in the PVA−PS positive friction layer of TENG. The short-circuit currents (d) and charge density (e) of TENG devices with a PVA layer of 2 μm thickness and PS friction layers of different thicknesses.

that the thicker the PVA layer becomes, the less the increment of the triboelectric charges will be. If we assume the charge quantity in the 4.7 μm thick PVA layer as the maximum charge capacity of the pure PVA friction layer, nearly 90% positive charges are stored in the space from the surface to 3.2 μm underneath it, and 99% positive charges are stored in the space from the surface to 4 μm underneath it. This means that an excess of thickness for the PVA friction layer will not supply more extra effective storage space for the triboelectric charges. This result is in agreement with the calculation results mentioned in our previous work.[40]

According to the above results, it can be found that the positive triboelectric charge rapidly decays to zero in the depth direction of the PVA layer. The regularly distributed positive charges in the PVA layer is basically the same as the electrons' in the pure polyvinylidene fluoride (PVDF) layer.[40] Therefore, it can be speculated that the introduction of CTL and CSBL, which has been proved effective in improving the electron storage capacity for the negative friction layer, may also benefit the improvement of the electron storage capacity of the PVA positive friction layer. To validate this, a polystyrene (PS) layer was selected as CSBL for PVA, and three different TENG devices were fabricated. The friction layer of TENG-A is composed of a surface PS layer with the thickness of 20 μm and a bottom PVA layer with the thickness of 5 μm. TENG-B's positive friction layer has only a PVA layer with a thickness of 5 μm. The friction layer of TENG-C is composed of a surface PVA layer with the thickness of 5 μm and a bottom PS layer with the thickness of 20 μm. The opposite friction layers of these three TENGs are all aluminum films. After operation for 30 min under the same driving conditions, the short-circuit current signals of these TENGs are gathered, as shown in Figure 2a. Figure 2b illustrates their corresponding charge capacity. In fact, PS is a kind of negative friction material for TENG with a stronger ability to capture electrons than aluminum. During the friction process between PS and aluminum, electrons will transfer from aluminum to PS, and the charge capacity of the PS−PVA composite friction layer in TENG-A is −0.78 nC/cm^2. By contrast, PVA will lose electrons when contacting with aluminum. The charge capacity of PVA friction layer in TENG-B is 0.73 nC/cm^2. However, the interesting thing is that when the PS layer is added between PVA and the electrode in TENG-C, the charge capacity of its composite layer is promoted to 2.1 nC/cm^2, which is 2.8 times as much as that in TENG-B with the pure PVA layer.

To explore the effect of CSBL, another 8 TENGs with different thicknesses were prepared. Their positive friction layers adopted the double-layer structure, as shown in Figure 2c. All of their surface layers are PVA with the thickness of 2 μm. The PS layer with different thicknesses from 3 to 20 μm is located between the PVA layer and electrode. Their negative friction layers are also aluminum films. Under the same driving conditions, the short-circuit currents of these 8 TENGs were gathered, as shown in Figure 2d, and the charge capacity of these PVA−PS layers are shown in Figure 2e. First, for the TENG with the PVA−PS composite layer, the charge capacity is 0.9 nC/cm^2 when the thickness of the composite layer is 5 μm (PVA layer is 2 μm and PS layer is 3 μm). With the increase of the PS layer's thickness, the charge capacity reveals a trend of rising first and becoming stable finally. The maximal charge capacity reaches 2.1 nC/cm^2 when the thickness of the composite layer is 22 μm (PVA layer is 2 μm, and PS layer is 20 μm). For the TENG with a pure PVA layer, the distribution trend of positive triboelectric charges is similar to that in the PVA−PS layer, but its maximal charge capacity is only 0.74 nC/cm^2. Second, for the PVA−PS composite layer, the storage depth of triboelectric charges is also greater than that for the pure PVA layer. In the composite friction layer, 90% positive charges are stored from the surface to a depth of 12 μm, as shown in Figure 2e. In the pure PVA layer, the corresponding thickness is only 3.2 μm (Figure 1c). Thus, it can be seen that PS CSBL indeed has great enhancing effect on the PVA positive friction layer.

DOI: 10.1021/acsaem.8b00530
ACS Appl. Energy Mater. 2018, 1, 2891−2897

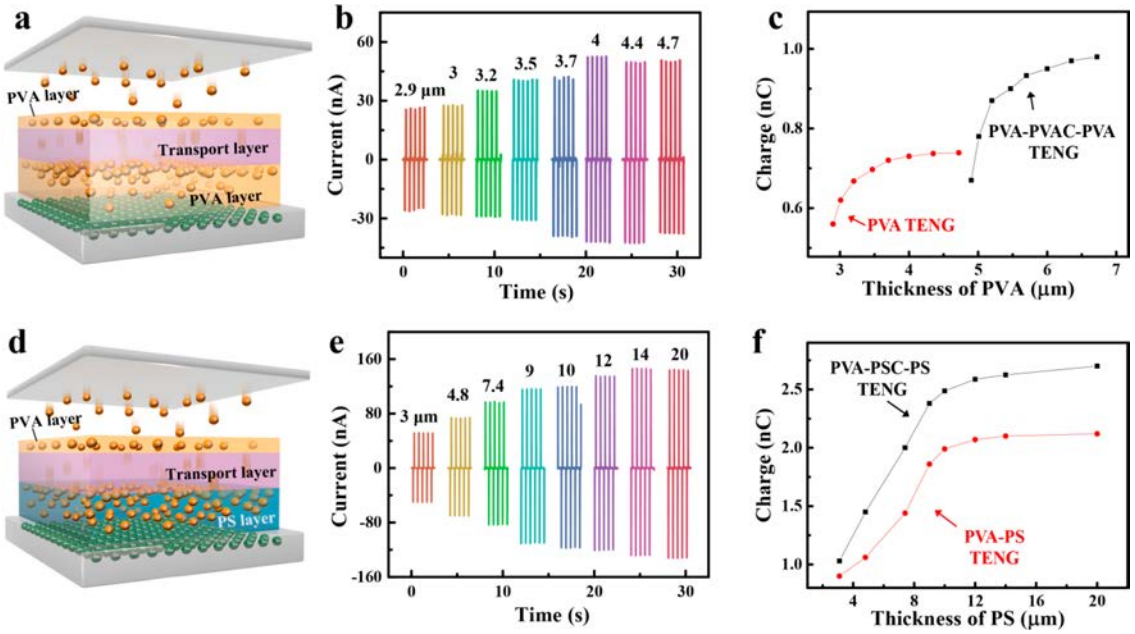

Figure 3. (a) Schematic of the transport process of PVA−PVAC−PVA positive friction layer of TENG. The short-circuit current (b) and charge capacity (c) of TENG with bottom PVA friction layers of different thicknesses while the devices' top PVA layers are all 2 μm and PVAC layers are 5 μm. (d) Schematic of the transport process of PVA−PSC−PS positive friction layer of TENG. The short-circuit currents (e) and charge capacity (f) of TENG with bottom PS friction layers of different thicknesses while the devices' top PVA layers are all 2 μm and PSC layers are 5 μm.

Low carrier mobility, low intrinsic carrier density, and abundant traps of the PS layer greatly reduce the triboelectric charge loss from electrode and extend the storage depth of the charge and increase the charge capacity of the whole friction layer.[40] In contrast, CTL can increase the charge capacity of the friction layer through increasing the triboelectric charge yield (TCY). For this, a reasonable explanation was given in the previous research: TCY, which can reflect how fast the charges will be transfused into the friction layer, is relevant not only to the materials of the friction layer and the driving conditions of TENG but also to the quantity of earlier entered charges. In other words, the pre-entered charges will hinder the subsequent triboelectric charges from entering into the friction layer. The function of CTL is to weaken the impediment of the new charges' entrance by transporting and taking part of the triboelectric charges far from the surface of the friction layer. To validate the effect of CTL on the positive friction layer, a PVA-doped 0.7 wt % carbon nanotubes (CNTs) (PVAC) layer was prepared first and then applied in the pure PVA friction layer to form a PVA−PVAC−PVA sandwich structure in the TENG. As shown in Figure 3a, the thickness of the PVA surface layer is kept constant at 2 μm, and the thickness of the PVAC middle layer is 5 μm. We adjusted the thickness of PVA bottom layer from 2.9 to 4.7 μm and then tested short-circuit currents of these devices. The short-circuit currents of this group of TENGs were gathered under the same driven conditions, as shown in Figure 3b. The charge capacities of these PVA−PVAC−PVA layers are shown with the black line in Figure 3c. Compared with TENG made of the pure PVA layer, though the relationship between the charge capacity and the total thickness of PVA layer has a similar variation trend, the maximum capacity and storage depth of the PVA−PVAC−PVA friction layer are increased obviously. That is because the increase of TCY breaks the original balance between the accumulation and loss of charges and makes the capacity−thickness curve move to the upper right. Likewise, a PS-doped 0.7 wt % CNTs (PSC) layer was prepared by applying the CTL to the PVA−PS structure. The new sandwich structure of the device is shown in Figure 3d. The surface layer is a 2 μm thick PVA layer; the middle layer is a 5 μm thick PSC layer, and the bottom layer is a PS CSBL ranging from 3 to 20 μm. From the output performance test, the short-circuit currents and charge capacity of this structure are shown in Figure 3e,f. The introduction of PSC layer brings an increase of 1.27 times to the charge capacity of the PS layer as the thickness of PS layer is 20 μm. It also can be found that the thicker the PS layer, the greater the influence of the CTL. This is because, for a PVA−PSC−PS TENG with a thicker PS layer, a greater proportion of positive charges was separated from the surface by CTL. That way, the function of the CTL certainly becomes more obvious. In general, compared with a pure PVA layer, the PVA−PSC−PS structure gives a factor of 3.7 improvement in the charge capacity of the friction layer (0.37 nC/cm^2 for the pure PVA layer and 2.7 nC/cm^2 for the composite layer).

The charge accumulation and dissipation process over time for three TENGs with different positive friction layer structures was tested afterward. The results of TENGs with pure PVA layer, PVA−PS layer, and PVA−PSC−PS layer are shown in Figure 4. It can be found that the introduced PS dramatically slows the decay rate of the accumulated charges (Figure 4b). For the pure PVA friction layer (Figure 4a), it takes 25 min for the triboelectric charges to decay to 1/e of its original level after the device stopped working, while the PVA−PS friction layer takes 26 h, and PVA−PSC−PS layer takes 7 h (Figure 4c). Here, the introduced PSC sublayer reduces the charge decay time significantly. This shows that a CTL can also accelerate the loss rate of the triboelectric charges while increasing the TCY. Therefore, the CTL is more suitable to work under the high-frequency and continuous driving conditions, such as sound waves. But for the low-frequency and irregular driving conditions, such as breeze or body motion, the PVA−PS structure should be preferred. Currently, the improving effect of

DOI: 10.1021/acsaem.8b00530
ACS Appl. Energy Mater. 2018, 1, 2891−2897

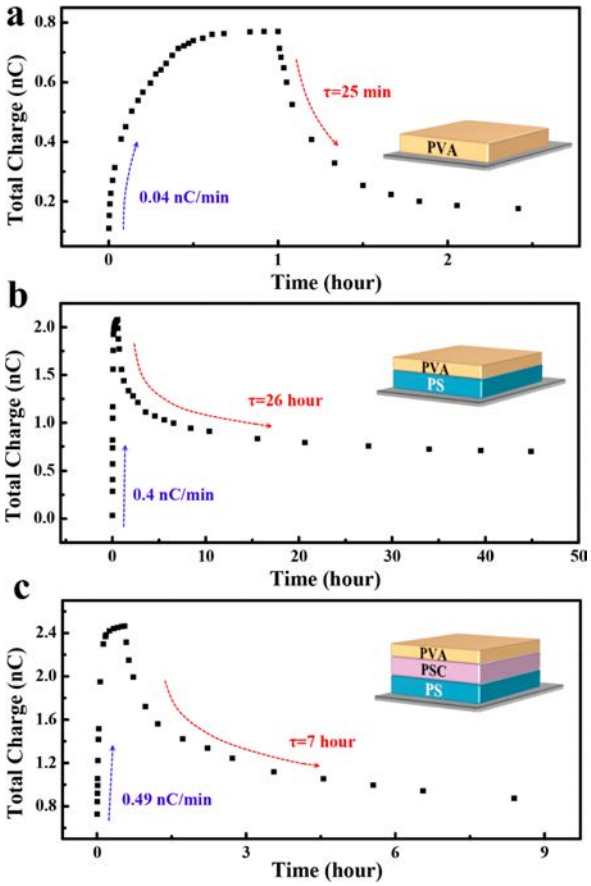

Figure 4. Accumulation process and decay process of the triboelectric charge for pure PVA TENG device (a), PVA−PS TENG device (b) and PVA−PSC−PS TENG device (c).

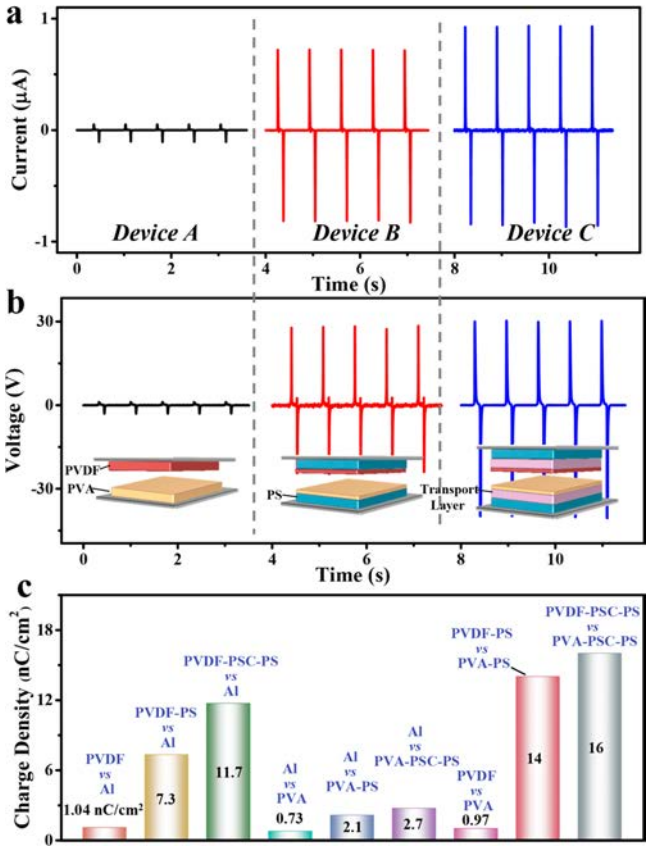

Figure 5. Short-circuit currents (a) and the voltage with 100 MΩ load resistance (b) of the TENG devices when the composite friction layers are applied in both the positive and negative friction layer. (c) The improvement effects of different composite friction layer structure.

CTL on TCY is reflected only from the experimental results now and still has no exact theoretical model to explain its internal mechanism. This is what we want to improve in follow-up work. In addition, for reducing the loss of the triboelectric charges, the introduced PS layer can also increase the charge accumulation rate. At the driving frequency of 1 Hz, the PVA layer needs 15 min to accumulate 80% of its maximum capacity, and the average accumulation rate is 0.04 nC/min. As for PVA−PS layer and PVA−PSC−PS layer, the corresponding time is 3.6 and 3.8 min, and the average charge accumulation rates are 0.4 and 0.49 nC/min. Therefore, the charge accumulation rates of the two composite positive friction layers are 10 times that of the pure PVA layer.

So far, we have already demonstrated the effect of CSBL and CTL on the negative[40] and positive friction layer. For the sake of analysis, we adopted aluminum film as the opposite friction layer in previous experiments. But actually, to improve the output performance of TENG further, the two functional sublayers may well be applied into the negative friction layer and positive friction layer at the same time. Based on this, three TENGs have been prepared. As shown in Figure 5b, TENG-A has a PVA positive friction layer and a PVDF negative friction layer both with thickness of 5 μm. TENG-B has a PVA−PS positive friction layer and a PVDF−PS negative friction layer, in which the thickness of PVA and PVDF are both 2 μm and the thickness of PS is 20 μm. In TENG-C, two PSC layers of 5 μm thickness were added in the friction layer based on the structure of TENG-B. The outputs of these TENGs are shown in Figure 5a,b. The triboelectric charge capacity of TENG-A is 0.97 nC/cm^2, and the capacity of TENG-B is 14 nC/cm^2; TENG-C earns a slightly higher charge capacity of 16 nC/cm^2. In summary, the triboelectric charge density can increase 14.4 times by adding CSBL in both the negative and positive friction layer and 16.5 times by building a CCL−CTL−CSBL three-layer structure in the two friction layers (Figure 5c).

■ CONCLUSION

In summary, we introduced CTL and CSBL into the positive friction layer of TENGs. CTL is formed by adding a small amount of CNTs into a PS or PVA layer. By slightly raising the conductivity of the positive friction layer, the triboelectric charges will transport through this layer quickly and hardly reside in it. This passageway for charge can help the entered triboelectric charges be far from the surface and reduce the repulsive force to the charges that will enter the friction layer later. CSBL is the PS layer that has low carrier mobility, low intrinsic carrier concentration, and rich defects. The TLCS applied in the positive friction layer can give a factor of 3.7 improvement in the charge capacity of TENG. By application of TLCS on both the positive and negative friction layers, the charge capacity of the TENG will improve 16.5 times. This approach greatly enhances the charge capacity of the friction layers and thus enhances the performance of the TENG.

■ METHODS

Preparation of the PVA and PS Solutions. In a 50 mL triangular flask, 2.0 g of PVA was mixed with 20.0 g of deionized water.

DOI: 10.1021/acsaem.8b00530
ACS Appl. Energy Mater. 2018, 1, 2891−2897

The solution was stirred at 80 °C for 3 h. In a 50 mL triangular flask, 3.0 g of PS was mixed with 8.0 g of *N,N*-dimethylformamide, then the mixture was stirred for 3 h to ensure the dissolution of PS. All reagents were analytically pure and used without any further purification.

Fabrication of TENG Devices. First, to fabricate the positive friction layer part of the TENG, a piece of glass slide with side length of 2.5 cm was prepared as substrate. Then, a piece of corresponding size aluminum foil was adhered on the surface of this substrate by double-sided tape. After that, the positive friction layers were prepared on the surface of aluminum foil by a spin coating method. When the spin speed of coating is adjusted from 500 to 4000 rpm, the thickness of the friction layer can be controlled easily. For the purpose of facilitating the comparison, all the different positive friction layers share the same one negative friction layer, which is composed of a glass substrate with side length of 1 cm and a piece of aluminum foil affixed to it.

■ AUTHOR INFORMATION

Corresponding Author

*E-mail: qinyong@xidian.edu.cn.

ORCID

Yong Qin: 0000-0002-6713-480X

Notes

The authors declare no competing financial interest.

■ ACKNOWLEDGMENTS

Research was supported by NSFC (Nos. 51322203, 51472111, and 51603162), Natural Science Foundation of Shaanxi Provincial Department of Education (No. 2017JQ5036), the National Program for Support of Top-notch Young Professionals, the Fundamental Research Funds for the Central Universities (No. lzujbky-2016-k02), NSFC (Grant No. BJ19016310004), the Fundamental Research Funds for the Central Universities (Grant No. JB181405; No. JBX171409; No. JB161401; No. JB161402).

■ REFERENCES

(1) Zou, Y.; Hu, X.; Ma, H.; Li, S. E. Combined State of Charge and State of Health Estimation over Lithium Ion Battery Cell Cycle Lifespan for Electric Vehicles. *J. Power Sources* **2015**, *273*, 793−803.

(2) Cui, N.; Wu, W.; Zhao, Y.; Bai, S.; Meng, L.; Qin, Y.; Wang, Z. L. Magnetic Force Driven Nanogenerators as a Noncontact Energy Harvester and Sensor. *Nano Lett.* **2012**, *12*, 3701−3705.

(3) Mao, Y.; Zhao, P.; Mcconohy, G.; Yang, H.; Tong, Y.; Wang, X. Sponge-Like Piezoelectric Polymer Films for Scalable and Integratable Nanogenerators and Self-Powered Electronic Systems. *Adv. Energy Mater.* **2014**, *4*, 1301624.

(4) Park, K. I.; Son, J. H.; Hwang, G. T.; Jeong, C. K.; Ryu, J.; Koo, M.; Choi, I.; Lee, S. H.; Byun, M.; Wang, Z. L. Highly Efficient, Flexible Piezoelectric PZT Thin Film Nanogenerator on Plastic Substrates. *Adv. Mater.* **2014**, *26*, 2514−2520.

(5) Hwang, G. T.; Park, H.; Lee, J. H.; Oh, S.; Park, K. I.; Byun, M.; Park, H.; Ahn, G.; Jeong, C. K.; No, K. Self-Powered Cardiac Pacemaker Enabled by Flexible Single Crystalline PMN-PT Piezoelectric Energy Harvester. *Adv. Mater.* **2014**, *26*, 4880−4887.

(6) Jeong, C. K.; Kim, I.; Park, K. I.; Oh, M. H.; Paik, H.; Hwang, G. T.; No, K.; Nam, Y. S.; Lee, K. J. Virus Directed Design of a Flexible $BaTiO_3$ Nanogenerator. *ACS Nano* **2013**, *7*, 11016−11025.

(7) Jeong, C. K.; Park, K. I.; Ryu, J.; Hwang, G. T.; Lee, K. J. Large-Area and Flexible Lead-Free Nanocomposite Generator Using Alkaline Niobate Particles and Metal Nanorod Filler. *Adv. Funct. Mater.* **2014**, *24*, 2620−2629.

(8) Jeong, C. K.; Park, K. I.; Son, J. H.; Hwang, G. T.; Lee, S. H.; Park, D. Y.; Lee, H. E.; Lee, H. K.; Byun, M.; Lee, K. J. Self-Powered Fully-Flexible Light-Emitting System Enabled by Flexible Energy Harvester. *Energy Environ. Sci.* **2014**, *7*, 4035−4043.

(9) Persano, L.; Dagdeviren, C.; Su, Y.; Zhang, Y.; Girardo, S.; Pisignano, D.; Huang, Y.; Rogers, J. A. High Performance Piezoelectric Devices Based on Aligned Arrays of Nanofibers of Poly (Vinylidenefluoride-Co-Trifluoroethylene). *Nat. Commun.* **2013**, *4*, 1633.

(10) Ramadoss, A.; Saravanakumar, B.; Lee, S. W.; Kim, Y. S.; Kim, S. J.; Wang, Z. L. Piezoelectric Driven Self Charging Supercapacitor Power Cell. *ACS Nano* **2015**, *9*, 4337−4345.

(11) Zi, Y.; Lin, L.; Wang, J.; Wang, S.; Chen, J.; Fan, X.; Yang, P. K.; Yi, F.; Wang, Z. L. Triboelectric Pyroelectric Piezoelectric Hybrid Cell for High Efficiency Energy Harvesting and Self-Powered Sensing. *Adv. Mater.* **2015**, *27*, 2340−2347.

(12) Beeby, S. P.; Torah, R.; Tudor, M.; Glynne-Jones, P.; O'Donnell, T.; Saha, C.; Roy, S. A Micro Electromagnetic Generator for Vibration Energy Harvesting. *J. Micromech. Microeng.* **2007**, *17*, 1257−1265.

(13) Galchev, T.; McCullagh, J.; Peterson, R.; Najafi, K. Harvesting Traffic-Induced Vibrations for Dtructural Health Monitoring of Bridges. *J. Micromech. Microeng.* **2011**, *21*, 104005.

(14) Mitcheson, P. D.; Green, T. C.; Yeatman, E. M.; Holmes, A. S. Architectures for Vibration Driven Micropower Generators. *J. Microelectromech. Syst.* **2004**, *13*, 429−440.

(15) Fan, F. R.; Tian, Z. Q.; Wang, Z. L. Flexible Triboelectric Generator. *Nano Energy* **2012**, *1*, 328−334.

(16) Yang, J.; Yang, F.; Zhao, L.; Shang, W.; Qin, H.; Wang, S.; Jiang, X.; Cheng, G.; Du, Z. Managing and Optimizing the Output Performances of a Triboelectric Nanogenerator by a Self-Powered Electrostatic Vibrator Switch. *Nano Energy* **2018**, *46*, 220.

(17) Cheng, G.; Zheng, H.; Yang, F.; Zhao, L.; Zheng, M.; Yang, J.; Qin, H.; Du, Z.; Wang, Z. L. Managing and Maximizing the Output Power of a Triboelectric Nanogenerator by Controlled Tip−Electrode Air-Discharging and Application for UV Sensing. *Nano Energy* **2018**, *44*, 208−216.

(18) Shang, W.; Gu, G. Q.; Yang, F.; Zhao, L.; Cheng, G.; Du, Z. L.; Wang, Z. L. A Sliding-Mode Triboelectric Nanogenerator with Chemical Group Grated Structure by Shadow Mask Reactive Ion Etching. *ACS Nano* **2017**, *11*, 8796.

(19) Cheng, G.; Lin, Z. H.; Lin, L.; Du, Z. L.; Wang, Z. L. Pulsed Nanogenerator with Huge Instantaneous Output Power Density. *ACS Nano* **2013**, *7*, 7383−7391.

(20) Cheng, G.; Lin, Z. H.; Du, Z.; Wang, Z. L. Simultaneously Harvesting Electrostatic and Mechanical Energies from Flowing Water by a Hybridized Triboelectric Nanogenerator. *ACS Nano* **2014**, *8*, 1932−9.

(21) Lin, L.; Xie, Y.; Niu, S.; Wang, S.; Yang, P. K.; Wang, Z. L. Robust Triboelectric Nanogenerator Based on Rolling Electrification and Electrostatic Induction at an Instantaneous Energy Conversion Efficiency of∼ 55%. *ACS Nano* **2015**, *9*, 922−930.

(22) Tang, W.; Jiang, T.; Fan, F. R.; Yu, A. F.; Zhang, C.; Cao, X.; Wang, Z. L. Liquid Metal Electrode for High Performance Triboelectric Nanogenerator at an Instantaneous Energy Conversion Efficiency of 70.6%. *Adv. Funct. Mater.* **2015**, *25*, 3718−3725.

(23) Zi, Y.; Lin, L.; Wang, J.; Wang, S.; Chen, J.; Fan, X.; Yang, P. K.; Yi, F.; Wang, Z. L. Triboelectric Pyroelectric Piezoelectric Hybrid Cell for High Efficiency Energy Harvesting and Self Powered Sensing. *Adv. Mater.* **2015**, *27*, 2340−2347.

(24) Cui, N.; Gu, L.; Liu, J.; Bai, S.; Qiu, J.; Fu, J.; Kou, X.; Liu, H.; Qin, Y.; Wang, Z. L. High Performance Sound Driven Triboelectric Nanogenerator for Harvesting Noise Energy. *Nano Energy* **2015**, *15*, 321−328.

(25) Gu, L.; Cui, N.; Liu, J.; Zheng, Y.; Bai, S.; Qin, Y. Packaged Triboelectric Nanogenerator with High Endurability for Severe Environments. *Nanoscale* **2015**, *7*, 18049−18053.

(26) Liu, J.; Cui, N.; Gu, L.; Chen, X.; Bai, S.; Zheng, Y.; Hu, C.; Qin, Y. A Three-Dimensional Integrated Nanogenerator for Effectively Harvesting Sound Energy from the Environment. *Nanoscale* **2016**, *8*, 4938−4944.

(27) Yang, J.; Chen, J.; Yang, Y.; Zhang, H.; Yang, W.; Bai, P.; Su, Y.; Wang, Z. L. Broadband Vibrational Energy Harvesting Based on a Triboelectric Nanogenerator. *Adv. Energy Mater.* **2014**, *4*, 1301322.

DOI: 10.1021/acsaem.8b00530
ACS Appl. Energy Mater. 2018, 1, 2891−2897

(28) Cui, N.; Liu, J.; Gu, L.; Bai, S.; Chen, X.; Qin, Y. Wearable Triboelectric Generator for Powering the Portable Electronic Devices. *ACS Appl. Mater. Interfaces* **2015**, *7*, 18225−18230.
(29) Wen, Z.; Chen, J.; Yeh, M. H.; Guo, H.; Li, Z.; Fan, X.; Zhang, T.; Zhu, L.; Wang, Z. L. Blow Driven Triboelectric Nanogenerator as an Active Alcohol Breath Analyzer. *Nano Energy* **2015**, *16*, 38−46.
(30) Wang, S.; Mu, X.; Wang, X.; Gu, A. Y.; Wang, Z. L.; Yang, Y. Elasto-Aerodynamics-Driven Triboelectric Nanogenerator for Scavenging Air Flow Energy. *ACS Nano* **2015**, *9*, 9554−9563.
(31) Quan, Z.; Han, C. B.; Jiang, T.; Wang, Z. L. Robust Thin Films-Based Triboelectric Nanogenerator Arrays for Harvesting Bidirectional Wind Energy. *Adv. Energy Mater.* **2016**, *6*, 1501799.
(32) Wang, X.; Wang, S.; Yang, Y.; Wang, Z. L. Hybridized Electromagnetic−Triboelectric Nanogenerator for Scavenging Air-Flow Energy to Sustainably Power Temperature Sensors. *ACS Nano* **2015**, *9*, 4553−62.
(33) Wang, S.; Mu, X.; Yang, Y.; Sun, C.; Gu, A. Y.; Wang, Z. L. Flow-Driven Triboelectric Generator for Directly Powering a Wireless Sensor Node. *Adv. Mater.* **2015**, *27*, 240.
(34) Zhong, X.; Yang, Y.; Wang, X.; Wang, Z. L. Rotating-Disk-Based Hybridized Electromagnetic-Triboelectric Nanogenerator for Scavenging Biomechanical Energy as a Mobile Power Source. *Nano Energy* **2015**, *13*, 771−780.
(35) Wang, S.; Wang, Z. L.; Yang, Y. A One-Structure-Based Hybridized Nanogenerator for Scavenging Mechanical and Thermal Energies by Triboelectric-Piezoelectric-Pyroelectric Effects. *Adv. Mater.* **2016**, *28*, 2881−2887.
(36) Wang, X.; Zhang, H.; Dong, L.; Han, X.; Du, W.; Zhai, J.; Pan, C.; Wang, Z. L. Self-Powered High-Resolution and Pressure-Sensitive Triboelectric Sensor Matrix for Real-Time Tactile Mapping. *Adv. Mater.* **2016**, *28*, 2896−2903.
(37) Jeong, C. K.; Baek, K. M.; Niu, S.; Nam, T. W.; Hur, Y. H.; Park, D. Y.; Hwang, G. T.; Byun, M.; Wang, Z. L.; Jung, Y. S. Topographically Designed Triboelectric Nanogenerator via Block Copolymer Self-Assembly. *Nano Lett.* **2014**, *14*, 7031−7038.
(38) Tang, W.; Zhang, C.; Han, C. B.; Wang, Z. L. Enhancing Output Power of Cylindrical Triboelectric Nanogenerators by Segmentation Design and Multilayer Integration. *Adv. Funct. Mater.* **2014**, *24*, 6684−6690.
(39) Zheng, Y.; Cheng, L.; Yuan, M.; Wang, Z.; Zhang, L.; Qin, Y.; Jing, T. An Electrospun Nanowire Based Triboelectric Nanogenerator and Its Application in a Fully Self-Powered UV Detector. *Nanoscale* **2014**, *6*, 7842−7846.
(40) Cui, N.; Gu, L.; Lei, Y.; Liu, J.; Qin, Y.; Ma, X.; Hao, Y.; Wang, Z. L. Dynamic Behavior of the Triboelectric Charges and Structural Optimization of the Friction Layer for a Triboelectric Nanogenerator. *ACS Nano* **2016**, *10*, 6131−6138.

DOI: 10.1021/acsaem.8b00530
ACS Appl. Energy Mater. 2018, 1, 2891−2897